


## RESEARCH ARTICLE

# Raman spectroscopy system for real-time diagnosis of clinically significant prostate cancer tissue

Suse J. van Breugel<sup>1,2,3</sup> | Irene Low<sup>4</sup> | Mary L. Christie<sup>4</sup> |  
Morgan R. Pokorny<sup>4,5</sup> | Ramya Nagarajan<sup>4,6</sup> | Hannah U. Holtkamp<sup>1,2</sup> |  
Komal Srinivasa<sup>5,6</sup> | Satya Amirapu<sup>6</sup> | Michel K. Nieuwoudt<sup>1,2,3,7</sup> |  
M. Cather Simpson<sup>1,2,3,7,8</sup> | Kamran Zargar-Shoshtari<sup>4,5,6</sup> | Claude Agueraray<sup>1,3,8</sup> 

<sup>1</sup>The Photon Factory, University of Auckland, Auckland, New Zealand

<sup>2</sup>School of Chemical Sciences, University of Auckland, Auckland, New Zealand

<sup>3</sup>The Dodd-Walls Centre for Photonic and Quantum Technologies, University of Otago, Dunedin, New Zealand

<sup>4</sup>Counties Manukau District Healthboard, Auckland, New Zealand

<sup>5</sup>Auckland District Healthboard, Auckland, New Zealand

<sup>6</sup>Faculty of Medical and Health Sciences, University of Auckland, Auckland, New Zealand

<sup>7</sup>The MacDiarmid Institute for Advanced Materials and Nanotechnology, Victoria University of Wellington, Wellington, New Zealand

<sup>8</sup>Department of Physics, University of Auckland, Auckland, New Zealand

## Correspondence

Claude Agueraray, University of Auckland, Auckland, New Zealand.  
Email: [c.agueraray@auckland.ac.nz](mailto:c.agueraray@auckland.ac.nz)

## Funding information

New Zealand Ministry of Business, Innovation and Employment (MBIE), Grant/Award Number: UOAX1806

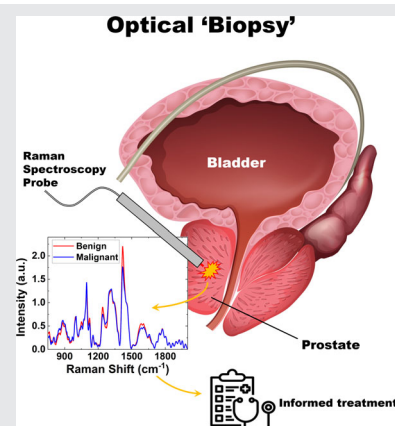
## Abstract

Prostate cancer (PCa) is a significant healthcare problem worldwide. Current diagnosis and treatment methods are limited by a lack of precise in vivo tissue analysis methods. Real-time cancer identification and grading could dramatically improve current protocols. Here, we report the testing of a thin optical probe using Raman spectroscopy (RS) and classification methods to detect and grade PCa accurately in real-time.

We present the first clinical trial on fresh ex vivo biopsy cores from an 84 patient cohort. Findings from 2395 spectra measured on 599 biopsy cores show high accuracy for diagnosing and grading PCa. We can detect clinically significant PCa from benign and clinically insignificant PCa with 90% sensitivity and 80.2% specificity. We also demonstrate the ability to differentiate cancer grades with 90% sensitivity and specificity  $\geq 82.8\%$ . This work demonstrates the utility of RS for real-time PCa detection and grading during routine transrectal biopsy appointments.

## KEYWORDS

biopsy cores, machine learning, prostate cancer, Raman spectroscopy, support vector machining, tissue optics



This is an open access article under the terms of the [Creative Commons Attribution-NonCommercial-NoDerivs](https://creativecommons.org/licenses/by-nc-nd/4.0/) License, which permits use and distribution in any medium, provided the original work is properly cited, the use is non-commercial and no modifications or adaptations are made.

© 2023 The Authors. *Journal of Biophotonics* published by Wiley-VCH GmbH.

## 1 | INTRODUCTION

Prostate cancer (PCa) is a significant healthcare problem in many western countries and particularly in New Zealand (NZ), where incidence and mortality rates are among the highest [1–3]. In NZ, around 4000 men are diagnosed each year, corresponding to an age-standardized incidence rate of 109.4 per 100 000 males [4]. The mortality rate due to PCa is comparably high, with more than 600 deaths registered each year [5]. This makes PCa the third-leading cause of all male cancer deaths and a significant healthcare problem in NZ. Following widespread use of prostate specific antigen (PSA) testing [6], we have observed an increased incidence of PCa diagnoses [4]. This, in turn, has led to concerns about overdiagnosis and overtreatment of some men with newly diagnosed PCa [7–9]. The more contemporary approach to PSA screening focuses on optimized patient selection. This is primarily achieved using PSA-based risk calculators and multiparametric magnetic resonance imaging (mpMRI) [10–13]. Long-term data demonstrates a relatively indolent course for low-risk (primary ISUP grade 1) PCa [14–17]. Therefore, in most clinical settings, only clinically significant PCa (ISUP 2 and higher) is of interest. Regardless of patient selection strategies, the only accepted standard for PCa diagnosis is tissue biopsy, either by transrectal or transperineal approach. Biopsy techniques have significantly improved, particularly with MRI-guided imaging and in-gantry or MRI-ultrasound fusion systems [18–21]. Regardless of the method, tissue must be extracted and analyzed for cancer diagnosis and grading. However, even with optimized utilization of mpMRI, the incidence of negative or clinically nonsignificant PCa is relatively high [22]. The rate of clinically significant PCa was 32% in the MRI-first study, (37%) in the PRECISION study, and (25%) in the 4M trial [23, 24]. In addition to the risk of diagnosing insignificant cancers, a saturation prostate biopsy is an invasive and risky procedure. The procedure could lead to side effects such as sepsis, hemorrhage, and urinary retention [25]. There is also always a risk of needing a repeat biopsy if the results come back inconclusive. This means the patient has to face the same risk and invasive procedure numerous times.

For these reasons, new approaches to the management of the disease are constantly being explored. An interesting treatment approach was recently suggested by Meissner et al., who performed radical prostatectomy procedures without biopsy [26]. This approach negates the well-known prostate biopsy morbidity issues and associated stress and apprehension from the patient. However, as explained by Modi and Eggenner [27], wide adoption of such a treatment strategy would require significant improvement of current noninvasive diagnostic techniques.

This project explores the use of Raman spectroscopy (RS) for real-time intraoperative tissue analysis to enhance PCa detection strategies further and minimize the number of biopsies required for disease diagnosis. This approach has the potential to significantly decrease the number of required biopsies and their associated morbidity while enabling accurate diagnosis. It could provide an alternative for developing new treatment options mentioned previously [26, 27]. RS is a powerful analytical technique that utilizes the inelastic scattering of light [28, 29]. RS is robust, minimally invasive, capable of label-free analysis, and efficiently implemented into a portable design. It has already been shown to have a high potential for diagnosing many cancers [30–33]. In recent years, it was proved it can accurately detect PCa on large tissue samples obtained from radical prostatectomies [34–36]. Aubertin et al. demonstrated 86% classification accuracy between cancer and healthy tissue on freshly excised prostates [34]. They differentiated benign tissue from various Gleason grades with sensitivities and specificities ranging between 73% and 91% [36]. Pinto et al. adapted a RS probe to a Da Vinci robot in a proof-of-concept demonstration. They showed its ability to differentiate prostatic from extraprostatic tissue with accuracy, sensitivity, and specificity of 91%, 90.5%, and 96%, respectively [35]. Most recently, Picot et al. [37] combined RS with electromagnetic tracking to detect PCa during transperineal biopsy procedures. Though their dataset was limited, they achieved 86% sensitivity and 72% specificity.

Here, we have conducted a clinical study to assess the utility of RS as a diagnostic tool during transrectal prostate biopsy procedures. We present our progress toward developing a thin handheld fiber optic probe that can detect clinically significant PCa in real-time using optical prostate biopsy. We perform RS measurements on fresh prostate biopsy cores seconds after collection and demonstrate that we can accurately classify benign from malignant tissue and identify various Gleason patterns. The fast measurement time (1–2 s), classification algorithm (2–3 s), and thin probe design are suitable for use with current biopsy tools and do not disrupt the clinical workflow. This makes the technique suitable for use during transrectal prostate biopsy procedures, which are carried out routinely, while transperineal biopsy procedures are generally more complex and could require general anesthetic.

## 2 | MATERIALS AND METHODS

### 2.1 | Patient consent

Biopsy-naïve men with elevated PSA who were scheduled for prostate biopsy based on standard clinical parameters

were included in the study. All biopsy procedures were performed at Manukau SuperClinic (Counties Manukau District Health Board, Auckland, New Zealand). All patients were adults that were able to give their own informed consent. This project has been approved by the New Zealand Health and Disability Ethics Committees (HDEC, Ethics Reference Number 20/NTB/308).

## 2.2 | Specimen handling and analysis

Participants underwent standard transrectal ultrasound (TRUS)-guided or MRI-Fusion guided transrectal biopsies using an 18-gauge biopsy needle. The excised biopsy cores were placed onto filter paper irrigated with saline (0.9% NaCl), separated per location. Any cores that were fragile or contained substantial amounts of blood were not included and immediately immersed in 10% neutral buffered formalin solution (NBF) for fixation. The included cores were kept hydrated in saline before measurement.

Acquisitions were performed inside a lightproof experiment box. The RS probe was lowered to approximately 1 mm above the specimen using a micrometer precision translation stage. The area of the tissue measured by the probe equates to approximately 2.14 mm<sup>2</sup>. Four spectra were measured at the same location on each biopsy core. Up to two cores per biopsy location were measured. After all the RS measurements were completed, the location was marked using red or black tissue marking dye (Bradley Davidson) (see Figure 1). The tissue marking dye was fixed onto the tissue using 5% acetic acid solution.

## 2.3 | Instrumentation

RS measurements were performed using a custom-made handheld fiber optic probe (EmVision LLC). The probe has an external diameter of 1.65 mm and is coupled to a 785 nm wavelength-stabilized laser operated at 20 mW at the probe tip (Innovative Photonic Solutions) to respect the maximum permissible exposure limit of 5.5 W/cm<sup>2</sup> as set in the Australia/New Zealand standards (AS/NZ S IEC 60825.1:2014). The probe consists of one excitation fiber (300 μm diameter) surrounded by 12 collection fibers with 200 μm diameter. It also comprises a set of filters to prevent excitation photons from entering the collection fibers and to cut out the Raman signal produced in the excitation fiber. The probe was coupled to a portable back-illuminated deep-depletion charge-coupled device camera for detection of the Raman scattered photons (iVac; Andor Technology) (see Figure 1C). The spectrometer was calibrated using a known Raman signature

of acetaminophen each time it was deployed. One output spectrum is the sum of 50 measurements of 200 ms. This was repeated four times for each location to obtain four spectra for each location. The system was controlled using Andor Solis software.

## 2.4 | Pathology reporting

Specimens were fixed using 10% NBF immediately after measurement completion. Samples were then transferred for routine assessment by experienced pathologists. The samples were paraffin embedded, hematoxylin and eosin (H&E) stained, and cut at a slice thickness of 4 μm. The pathology of the tissue at the location of the tissue dye was determined using microscopy assessment at a combination of ×40, ×100, ×200, and ×400 magnification. For each core, three serial H&E-stained sections were assessed. When necessary, three more serial sections were assessed or immunohistochemistry stains were used for further assessment (high molecular weight cytokeratin and α-methacyl-CoA racemase).

Cores with a uniform pattern within the studied inked area were reported. The Gleason pattern was recorded in case of malignancy. The Gleason grading system was first described by Gleason et al. [38] in 1974 and is based on architectural differences in tumor cells. The Gleason pattern can help clinicians determine the tumor's aggressiveness and decide on treatment options. The regions in the tissue are assigned a Gleason pattern between 1 and 5, with 1 being the least aggressive or low-risk and 5 being the most aggressive or high-risk. The most prevalent grade and the highest secondary grade are combined into an ISUP grade group. There are five ISUP grade groups: ISUP1 = Gleason patterns 3 + 3, ISUP2 = Gleason patterns 3 + 4, ISUP3 = Gleason patterns 4 + 3, ISUP4 = Gleason patterns 4 + 4 and ISUP5 = Gleason patterns 4 + 5 and higher [39]. Examples of benign and malignant biopsy cores within the inked area are shown in Figure 2. In this study, the pathologist reported single Gleason patterns as the observed area was small. The ISUP grading system is mentioned when the clinical significance of the malignancy is assessed. In case of uncertainty within the reported area, the core was removed from the study.

## 2.5 | Data processing and analysis

Before analyzing the spectra, Raman peaks are isolated from background noise and system noise (etaloning effects) using an in-house Matlab signal processing code. Cosmic rays are removed from the spectra using a



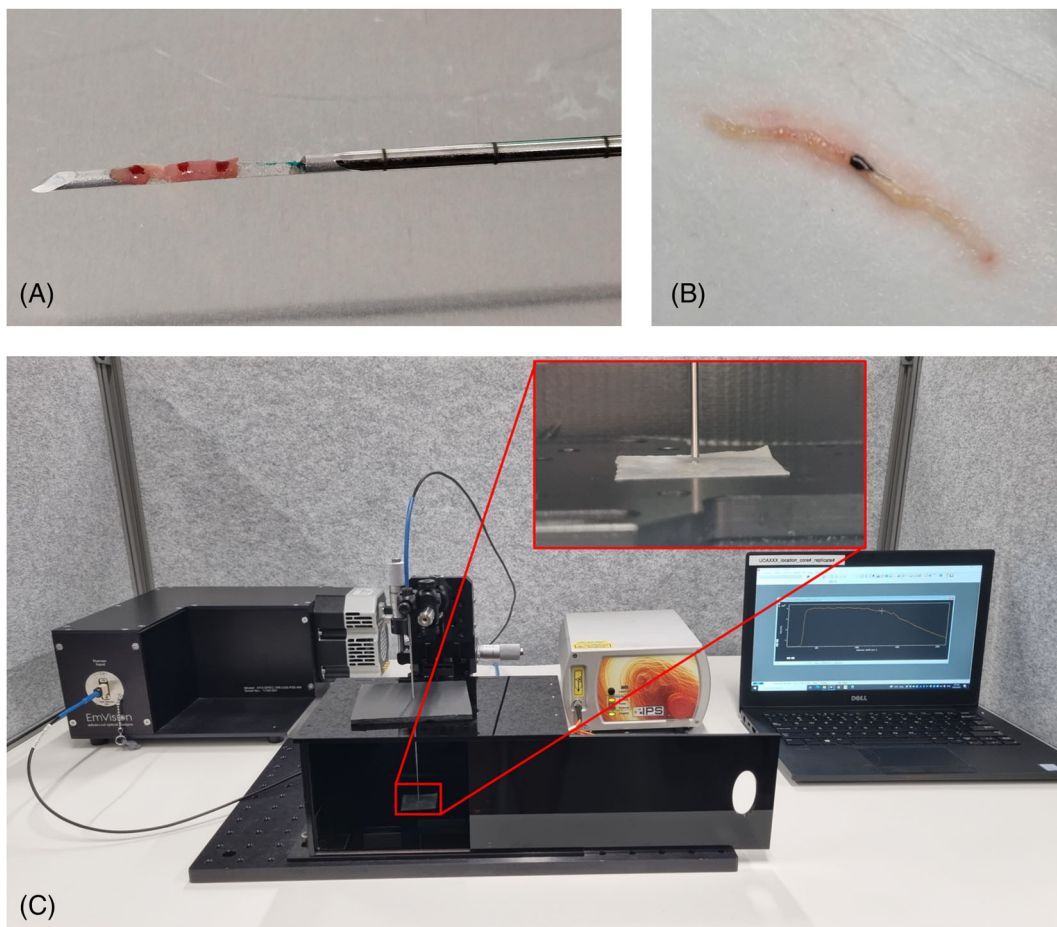


**FIGURE 1** (A) Marking of a core inside an 18 gauge biopsy needle with red tissue dye during study preparation. (B) Measurement location marked with black tissue dye on a prostate biopsy core placed on filter paper during the study. (C) Portable Raman apparatus used for the study.

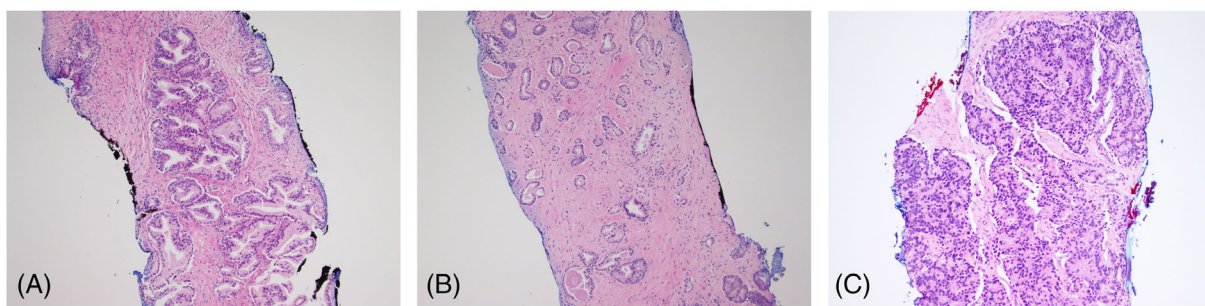


**FIGURE 2** Microscope histology slides of (A) benign biopsy core, (B) malignant biopsy core (Gleason pattern 3), (C) malignant biopsy core (Gleason pattern 4) marked with black or red tissue dye.

modified  $Z$  score and the median absolute deviation shown in Equations (1) and (2). After removal of the cosmic rays, the deleted data points are recalculated using a six-point moving average window. Etaloning effects result from undesired resonators in the probe in which reflected light interferes with incoming light to produce a ripple with slowly varying frequency across

the Raman spectrum [40]. Removal of this ripple is implemented in several steps. A “pure” ripple spectrum specific to this probe is acquired using a highly fluorescent sample. A scaled ripple spectrum is then removed from each Raman spectrum. Calculation of the scaling ratio for each Raman spectrum is done in a low Raman activity region. Finally, the remaining baseline is

removed using standard asymmetric least squares smoothing.

$$Z_i = \frac{0.6745(x_i - \bar{X})}{\text{MAD}}, \quad (1)$$

$$\text{MAD} = \text{median} |x_i - \bar{X}|. \quad (2)$$

After preprocessing the spectra, multivariate statistical analysis was carried out using Matlab (MathWorks) and PLS Toolbox (Eigenvector Research Inc). Principal component analysis (PCA) decomposition was used to explore relevant biomarkers in the Raman spectra. Partial least squares-discriminant analysis (PLS-DA) was used as a classification technique. For PLS-DA, the data was preprocessed using mean-centering, and Venetian blinds was used for leave-one-patient-out cross-validation. Variable selection was performed using the relevant biomarkers found in PCA and using automated variable selection by PLS Toolbox. External validation was performed by randomly splitting the data set in 75% training set and 25% validation set. Repeat measurements (the four spectra acquired at the same location on each biopsy core) were kept together. Classification performance was assessed by computing receiver operating characteristic (ROC) curves and obtaining sensitivity, specificity, and area under the curve (AUC) values. The reported values for these parameters correspond to the point on the ROC curve closest to the upper left corner of the graph. Support vector machining (SVM) classification using a radial basis function and optimized cost and gamma parameters was trialed to improve classification results further. The cost parameter was optimized by choosing nine values between 0.001 and 100. This parameter represents the penalty that is associated with errors in the calibration set where higher cost values lead to narrower margins between classes. The gamma parameter was ranged using nine values between  $10^{-6}$  and 10 and decides the shape of the hyperplane that separates the data. The SVM classification model tested all 81 combinations of cost and gamma parameters. The final parameter selection was based on a compromise between achieving good classification output while taking caution not to over-fit the calibration data by letting high gamma parameters distort the shape of the hyperplane. This meant that the final parameter selection was not necessarily the combination with the best classification outcome.

### 3 | RESULTS

In total, 84 men underwent biopsy, 31 patients underwent TRUS-guided biopsy, 53 patients underwent 3D

TABLE 1 Patient and tumor characteristics.

No. of patients	84
Patient age, mean (range), years	66 (48–85)
PSA level, mean (range), ng/mL	13.78 (0.2–120)
Ethnicity, No.	
NZ European	47
Other	37
Type of procedure, No.	
TRUS guided	31
3D semi-robotic MRI and TRUS fusion guided	53
No. of specimen	639
Pathology, No.	
Benign	450
Malignant	149
Gleason pattern, No.	
3	97
4	49
5	3

Abbreviations: MRI, magnetic resonance imaging; TRUS, transrectal ultrasound.

Semi-Robotic MRI and TRUS Fusion (Artemis; Innomedicus) guided biopsy. The average age of the 84 participants included in this study was 66 years old. The median PSA level of all participants was 13.78 ng/mL. In total, 2555 spectra were taken from 639 biopsy cores. On average, approximately seven biopsy cores were measured per patient. Ninety-four percent of cores were reported, while 6% were not reported as the marked spot could not be visualized by the pathologists. The spectra corresponding to the unreported cores were excluded from the study. For the reported cores, 75% were benign and 25% were malignant. Of the malignant biopsy cores, 65% were Gleason pattern 3, 33% were Gleason pattern 4, and 2% were Gleason pattern 5. Altogether 2395 spectra were included in the study (1799 were benign and 596 were malignant). The patient data and tumor statistics are summarized in Table 1.

#### 3.1 | Classification of significant and nonsignificant cancer tissue

On the included 2395 spectra, exploratory analyses using PCA scores and loadings plots were used to find relevant biomarkers for differentiating benign and malignant tissue. These are displayed in Figure 3A alongside the averaged benign and malignant (Gleason pattern 4) spectra.

An extended list of the relevant biomarkers can be found in Table 2.

Using PLS-DA classification, 90% sensitivity and 80.2% specificity were achieved for diagnosing clinically significant cancers. Specifically, we classify Gleason patterns 4 and 5 (ISUP grade 2 and higher) against benign tissue and nonsignificant cancers (Gleason pattern 3, ISUP grade 1) (see Figure 4A,B). SVM classification found a 72% sensitivity and 98.9% specificity.

### 3.2 | Classification of various Gleason patterns

Of the 596 malignant spectra included in this study, 388 were Gleason pattern 3, 196 were Gleason pattern 4, and 12 were Gleason pattern 5. Because of the relatively small sample size of Gleason pattern 5 spectra (only originating from two patients), these were excluded from the current data set. PLS-DA was performed to classify different Gleason patterns as described earlier for clinically significant cancers. The classification model to separate all types of cancers (ISUP grades 1–5) against benign tissue yielded lower performance with an optimum result of 63.1% sensitivity and 84.8% specificity corresponding to an AUC of 0.78. Similar performance was reached to classify Gleason pattern 3 alone against benign tissue with an AUC of 0.77.

Using SVM classification, the optimized performance was improved to 76.2% sensitivity and 96.6% specificity. The classification performance improves notably for clinically significant cancers. To compare the ability of our model to classify various tissue types or cancer grades, we calculated the corresponding specificity for a sensitivity of 90%. With these settings, we can classify Gleason pattern 4 from Gleason pattern 3 with 90% sensitivity and 82.8% specificity. This corresponds to an AUC of 0.91 as can be seen in Figure 4C,D. Optimized settings translate to an accuracy of 82.6% and a precision of 74.1% to diagnose Gleason pattern 4 against Gleason pattern 3. The sensitivity and specificity for distinguishing Gleason pattern 4 from benign tissue were 90% and 85.3% with an AUC of 0.93 (see Figure 4E,F). Finally, when Gleason pattern 5 spectra were included in the data set, they could be separated from Gleason patterns 3 and 4 with both sensitivity and specificity above 90%. However, as mentioned earlier, the sample size should be increased for this result to be significant. Using SVM classification, the optimized sensitivity and specificity for diagnosing Gleason pattern 4 against Gleason pattern 3 were improved to 77.0% and 92.0%. Likewise, these parameters also improved for distinguishing Gleason pattern 4 from benign tissue with a sensitivity and a specificity of 93.8% and 100%, respectively.

The differences in the spectra of Gleason pattern 3 and Gleason pattern 4 tissues can be observed in

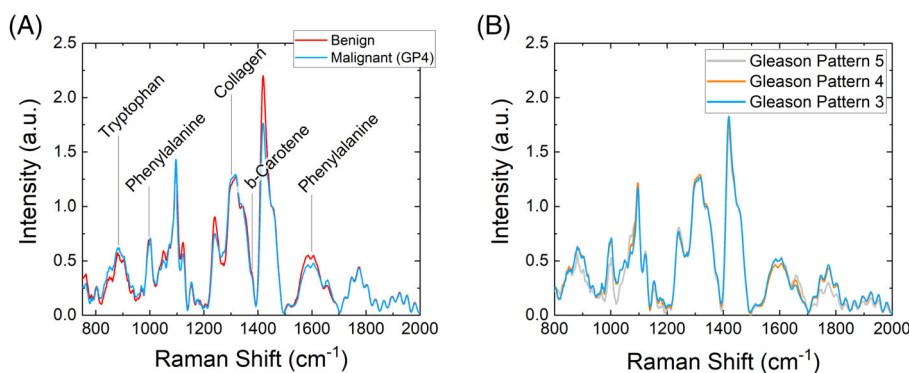


FIGURE 3 (A) Averaged benign and Malignant (Gleason pattern 4) spectra. (B) Averaged Gleason patterns 3, 4, and 5 spectra.

TABLE 2 Biomarkers found for benign and malignant PCa tissue by exploratory PCA using the scores and loadings plots.

Band (cm <sup>-1</sup> )	Molecular bond	Molecular species	Molecule	Dominant class
881	CH <sub>2</sub>	Proteins	Tryptophan	Malignant
1307	CH <sub>2</sub> /CH <sub>3</sub>	Proteins, lipids	Collagen	Malignant
1310	CH <sub>2</sub>	Protein	Collagen	Malignant
1396	CH <sub>2</sub>	Lipids	β-Carotene	Benign
1583	C=C	Proteins	Phenylalanine	Malignant
1602	C=C	Proteins	Phenylalanine, tyrosine, tryptophan	Malignant

Abbreviations: PCa, prostate cancer; PCA, principal component analysis.

**FIGURE 4** Receiver operating characteristic curves for validated partial least squares-discriminant analysis (A, C, E) and support vector machining (B, D, F) classifications of clinically significant prostate cancer (ISUP  $\geq 2$ ) versus benign and ISUP grade 1 tissues (A, B); Gleason pattern 4 versus Gleason pattern 3 tissues (C, D); and Gleason pattern 4 versus benign tissues (E, F). GP, Gleason pattern.

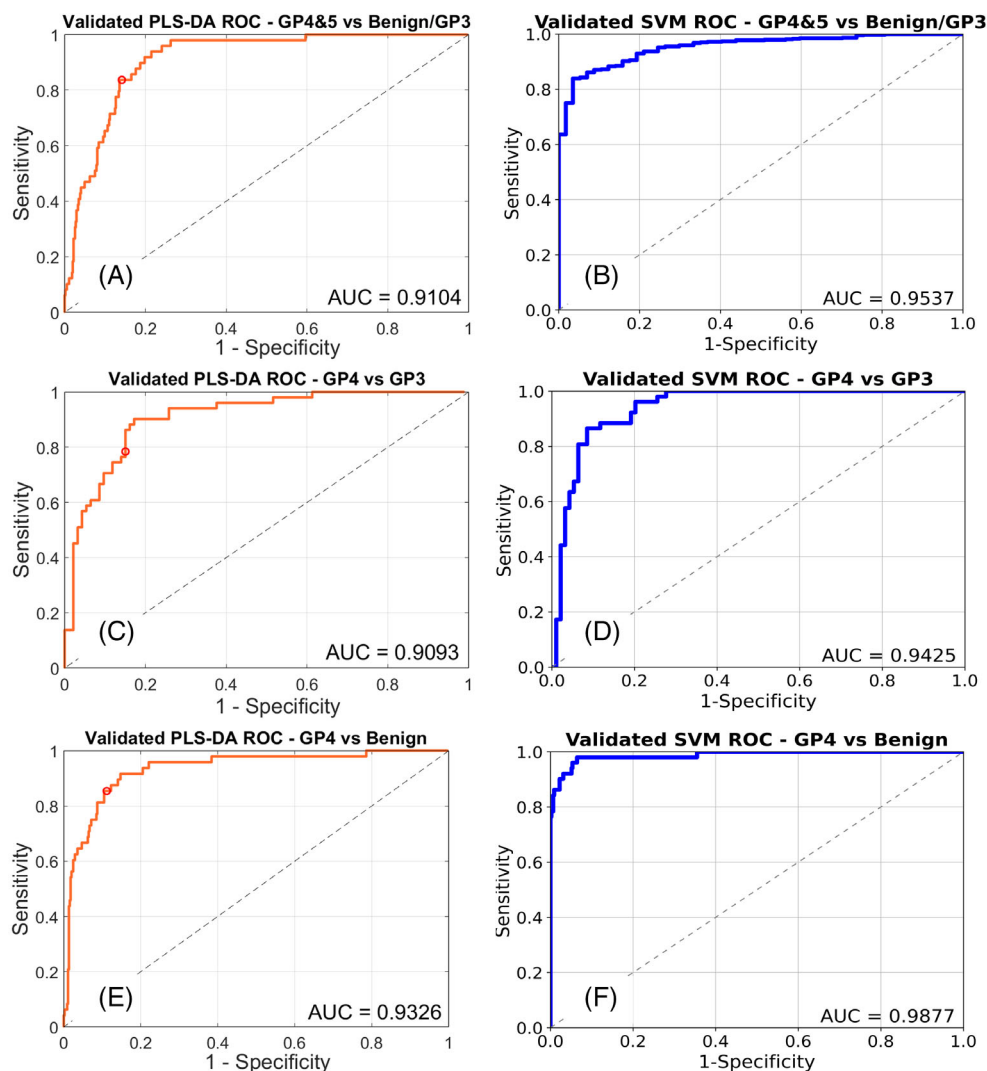


Figure 3B. The phenylalanine protein ( $1600\text{ cm}^{-1}$  peak) plays an important role in the classification of these two tissue types.

## 4 | DISCUSSION

Applying the current standard of care in this study, (38%) of TRUS patients had no evidence of malignancy (13%) or had clinically nonsignificant cancer (ISUP grade 1) (25%). Similar statistics are observed for 49% of ARTEMIS patients who had no evidence of malignancy (17%) or were diagnosed with ISUP grade 1 (32%). In vivo, real-time analysis of prostate tissue could help minimize these high numbers of negative biopsies.

Here, we present the first reported validated PLS-DA and SVM models of classification between benign and malignant prostate tissue, as well as classification between Gleason patterns 3, 4, and 5 malignant prostate tissue, using core biopsy samples obtained from transrectal biopsy

procedures. Several of the biomarkers identified are in accordance with recent literature [34, 36, 41]. A RS study on blood samples from healthy patients and PCa patients showed similar findings. For example, PCa samples were found to have decreased contributions for  $\beta$ -carotene and increased contributions of phenylalanine and tryptophan [42]. Our results also show that  $\beta$ -carotene had stronger scores for benign tissue. It has been found that  $\beta$ -carotene levels might decrease in cancer conditions, and  $\beta$ -carotene intake has also been correlated with reduced cancer risk for breast, colorectal, and ovarian cancers [43]. The higher scores for proteins and lipids for malignant tissue can be associated with increased metabolic activity and cell proliferation in cancer tissues [44].

The present results demonstrate the ability of the technique to accurately detect and classify clinically significant cancers. With the inclusion of all cancer patterns (ISUP grades 1–5), we can distinguish benign prostate tissue from malignant prostate tissue with an AUC of 0.78. The lower sensitivity of detection is due to the inclusion



of cores with a reported Gleason pattern 3 whose tissue structure and biochemical composition is closer to benign tissue compared to higher-grade cancers. This favors a more accurate detection of higher-grade cancers. As shown, significantly better classification was achieved for the identification of clinically significant cancers (Gleason 4) against benign tissue and against Gleason 3 with an AUC >0.91 in both cases, and a sensitivity of at least 90% was achieved with corresponding specificity >82.8%. Finally, Gleason pattern 5 was also well separated from Gleason patterns 3 and 4, however, more data is required for this result to be statistically significant. In all cases, SVM yielded excellent results for the classification of clinically significant cancers (GP4) against benign tissue with sensitivity higher than 90% and with specificity reaching 100%. These are the highest reported to date. These findings suggest that higher Gleason patterns have more significant biochemical differences from benign tissue, making it easier to differentiate them by RS. We suggest that this difference originates from the fact that higher-grade malignant tissue contains significantly less healthy tissue between cancer cells leading to more significant biochemical differences and more defined key biomarkers, thus enabling higher detection accuracy. Furthermore, higher-grade malignant tissue has more significant differences from benign tissue with regard to biochemical composition and tissue structure. These findings, in line with data obtained from postprostatectomy specimens using a macroscopic handheld RS probe where the AUC improved with each increasing Gleason pattern [36], confirm that PCa grading can be achieved in clinical settings using a minimally invasive probe.

## 5 | CONCLUSION

In conclusion, this study on a large patient cohort enabled the acquisition of an extensive data set and increased classification accuracy. It shows that, for the first time, both benign and malignant prostate tissue as well as different Gleason patterns can be accurately discriminated in small tissue samples (i.e., biopsy cores) using RS. The results presented herein for the classification of various PCa grades report the highest AUC to date. The ability of the technique to accurately diagnose cancers of ISUP grade 2 and higher using a hand-held probe with ultrashort measurement times (a few seconds) is extremely promising as it shows it can be applied for efficient intraoperative detection of high-risk and clinically significant cancers. The short integration time and thin probe design used to perform measurements make this technique suitable for translation into in vivo application during routine transrectal biopsies that do not

require general anesthetic. This method would help reduce the need for a saturation biopsy strategy with its well-known side effects.

## ACKNOWLEDGMENTS

The authors would like to thank Ariane Araquel-Lacamiento, Jejo Gotardo, and Jules Mudford from Counties Manukau District Health Board for their tireless effort and support during our data collection at Manukau SuperClinic and Eric Marple from EmVision LLC for the fabrication of our fiber optic probes. This project was funded by the New Zealand Ministry of Business, Innovation and Employment (MBIE) on an Endeavour Smart Idea grant, grant number UOAX1806. Open access publishing facilitated by The University of Auckland, as part of the Wiley - The University of Auckland agreement via the Council of Australian University Librarians.

## CONFLICT OF INTEREST STATEMENT

The authors declare no conflicts of interest.

## DATA AVAILABILITY STATEMENT

The data that support the findings of this study are available from the corresponding author upon reasonable request

## ORCID

Claude Agueraray  <https://orcid.org/0000-0001-5300-9920>

## REFERENCES

- [1] J. Ferlay, M. Ervik, F. Lam, M. Colombet, L. Mery, M. Pineros, A. Znaor, I. Soerjomataram, F. Bray, *Global Cancer Observatory: Cancer Today*, International Agency for Research on Cancer, Lyon, France **2020**. <https://gco.iarc.fr/today/home>
- [2] P. Rawla, *World J. Oncol.* **2019**, *20*, 63.
- [3] M. B. Culp, I. Soerjomataram, J. A. Efstathiou, F. Bray, A. Jemal, *Eur. Urol.* **2020**, *77*, 38.
- [4] New Zealand Ministry of Health, New Cancer Registrations 2019, **2021**. <https://www.health.govt.nz/publication/new-cancer-registrations-2018>
- [5] New Zealand Ministry of Health, Cancer: Historical Summary 1948–2017, **2020**. <https://www.health.govt.nz/publication/cancer-historical-summary-1948-2017>
- [6] B. Matti, K. Zargar-Shoshtari, *Urol. Oncol.: Semin. Orig. Invest.* **2020**, *38*, 393.
- [7] D. Ilic, M. Djulbegovic, J. H. Jung, E. C. Hwang, Q. Zhou, A. Cleves, T. Agoritsas, P. Dahm, *BMJ* **2018**, *362*, k3519.
- [8] R. M. Martin, J. L. Donovan, E. L. Turner, C. Metcalfe, G. J. Young, E. I. Walsh, J. A. Lane, S. Noble, S. E. Oliver, S. Evans, J. A. C. Sterne, P. Holding, Y. Ben-Shlomo, P. Brindl, N. J. Williams, E. M. Hill, S. Y. Ng, J. Toole, M. K. Tazewell, L. J. Hughes, C. F. Davies, J. C. Thorn, E. Down, G. D. Smith, D. E. Neal, F. C. Hamdy, J. Donovan, D. Neal, F. Hamdy, CAP Trial Group, *JAMA, J. Am. Med. Assoc.* **2018**, *319*, 883.



- [9] M. J. Barry, L. H. Simmons, *Med. Clin. North Am.* **2017**, *101*, 787.
- [10] N. Pereira-Azevedo, L. Osório, A. Fraga, M. J. Roobol, *JMIR Cancer* **2017**, *3*, e1.
- [11] J. Hippisley-Cox, C. Coupland, *Br. J. Gen. Pract.* **2021**, *71*, e364.
- [12] D. F. Osses, A. R. Alberts, G. C. F. Bausch, M. J. Roobol, *Transl. Androl. Urol.* **2018**, *7*, 27.
- [13] A. Jalali, R. W. Foley, R. M. Maweni, K. Murphy, D. J. Lundon, T. Lynch, R. Power, F. O'Brien, K. J. O'Malley, D. J. Galvin, G. C. Durkan, T. Brendan Murphy, R. William Watson, *BMC Med. Inf. Decis. Making* **2020**, *20*, 148.
- [14] S. E. Eggener, A. Berlin, A. J. Vickers, G. P. Paner, H. Wolinsky, M. R. Cooperberg, *J. Clin. Oncol.* **2022**, *40*, 3110.
- [15] C. V. Labbate, G. P. Paner, S. E. Eggener, *World J. Urol.* **2022**, *40*, 15.
- [16] A. Offermann, S. Hohensteiner, C. Kuempers, J. Ribbat-Idel, F. Schneider, F. Becker, M. C. Hupe, S. Duensing, A. S. Merseburger, J. Kirfel, M. Reischl, V. Lubczyk, R. Kuefer, S. Perner, *Front. Med.* **2017**, *4*, 157.
- [17] H. Lopor, N. M. Donin, *Oncology* **2014**, *28*, 16.
- [18] B. K. Park, *Cancers* **2021**, *13*, 5647.
- [19] J. J. Fütterer, A. Briganti, P. De Visschere, M. Emberton, G. Giannarini, A. Kirkham, S. S. Taneja, H. Thoeny, G. Villeirs, A. Villers, *Eur. Urol.* **2015**, *68*, 1045.
- [20] M. Pokorny, B. Kua, R. Esler, J. Yaxley, H. Samaratunga, N. Dungleon, T. Gianduzzo, G. Coughlin, R. Holt, B. Laing, D. Ault, N. Brown, R. Parkinson, L. Thompson, *World J. Urol.* **2019**, *37*, 1263.
- [21] M. R. Pokorny, M. de Rooij, E. Duncan, F. H. Schröder, R. Parkinson, J. O. Barentsz, L. C. Thompson, *Eur. Urol.* **2014**, *66*, 22.
- [22] L. Boesen, N. Nørgaard, V. Løgager, I. Balslev, H. S. Thomsen, *Urology* **2017**, *110*, 154.
- [23] O. Rouvière, P. Puech, R. Renard-Penna, M. Claudon, C. Roy, F. Mège-Lechevallier, M. Decaussin-Petrucci, M. Dubreuil-Chambardel, L. Magaud, L. Remontet, A. Ruffion, M. Colombel, S. Crouzet, A. M. Schott, L. Lemaitre, M. Rabilloud, N. Grenier, MRI-FIRST Investigators, *Lancet Oncol.* **2019**, *20*, 100.
- [24] V. Kasivisvanathan, A. S. Rannikko, M. Borghi, V. Panebianco, L. A. Mynderse, M. H. Vaarala, A. Briganti, L. Budäus, G. Hellawell, R. G. Hindley, M. J. Roobol, S. Eggener, M. Ghei, A. Villers, F. Bladou, G. M. Villeirs, J. Viridi, S. Boxler, G. Robert, P. B. Singh, W. Venderink, B. A. Hadaschik, A. Ruffion, J. C. Hu, D. Margolis, S. Crouzet, L. Klotz, S. S. Taneja, P. Pinto, I. Gill, C. Allen, F. Giganti, A. Freeman, S. Morris, S. Punwani, N. R. Williams, C. Brew-Graves, J. Deeks, Y. Takwoingi, M. Emberton, C. M. Moore, *N. Engl. J. Med.* **2018**, *378*, 1767.
- [25] B. Berry, M. G. Parry, A. Sujenthiran, J. Nossiter, T. E. Cowling, A. Aggarwal, P. Cathcart, H. Payne, J. van der Meulen, N. Clarke, *BJU Int.* **2020**, *126*, 97.
- [26] V. H. Meissner, I. Rauscher, K. Schwamborn, J. Neumann, G. Miller, W. Weber, J. E. Gschwend, M. Eiber, M. M. Heck, *Eur. Urol.* **2022**, *82*, 156.
- [27] P. K. Modi, S. E. Eggener, *Eur. Urol.* **2022**, *82*, 161.
- [28] Z. Movasaghi, S. Rehman, I. U. Rehman, *Appl. Spectrosc. Rev.* **2007**, *42*, 493.
- [29] C. Krafft, J. Popp, *Anal. Bioanal. Chem.* **2015**, *407*, 699.
- [30] N. M. Ralbovsky, I. K. Lednev, *Spectrochim. Acta, Part A* **2019**, *219*, 463.
- [31] K. Kong, C. Kendall, N. Stone, I. Notingher, *Adv. Drug Delivery Rev.* **2015**, *89*, 121.
- [32] W. Wang, J. Zhao, M. Short, H. Zeng, *J. Biophotonics* **2015**, *545*, 527.
- [33] E. Upchurch, M. Isabelle, G. R. Lloyd, C. Kendall, H. Barr, *Expert Rev. Mol. Diagn.* **2018**, *18*, 245.
- [34] K. Aubertin, J. Desroches, M. Jermyn, V. Q. Trinh, F. Saad, D. Trudel, F. Leblond, *Biomed. Opt. Express* **2018**, *9*, 4294.
- [35] M. Pinto, K. C. Zorn, J. P. Tremblay, J. Desroches, F. Dallaire, K. Aubertin, E. Marple, C. Kent, F. Leblond, D. Trudel, F. Lesage, *J. Biomed. Opt.* **2019**, *24*, 025001.
- [36] K. Aubertin, V. Q. Trinh, M. Jermyn, P. Baksic, *BJU Int.* **2018**, *122*, 326.
- [37] F. Picot, R. Shams, F. Dallaire, G. Sheehy, T. Trang, D. Grajales, M. Birlea, D. Trudel, C. Ménard, S. Kadoury, F. Leblond, *J. Biomed. Opt.* **2022**, *27*, 095003.
- [38] D. F. Gleason, G. T. Mellinger, L. J. Ardving, *J. Urol.* **1974**, *111*, 58.
- [39] J. I. Epstein, L. Egevad, M. B. Amin, B. Delahunt, J. R. Srigley, P. A. Humphrey, *Am. J. Surg. Pathol.* **2016**, *40*, 244.
- [40] J. Holly, L. A. Butler, B. Bird, G. Cinque, K. Curtis, J. Dorney, K. Esmonde-white, N. J. Fullwood, B. Gardner, P. L. Martin-Hirsch, M. J. Walsh, M. R. Mcainsh, N. Stone, F. L. Martin, *Nat. Protoc.* **2016**, *11*, 664.
- [41] L. Silveira Jr., K. R. M. Leite, F. L. Silveira, M. Srougi, M. T. T. Pacheco, R. A. Zângaro, C. A. Pasqualucci, *Lasers Med. Sci.* **2014**, *29*, 1469.
- [42] D. K. R. Medipally, D. Cullen, V. Untereiner, G. D. Sockalingum, A. Maguire, T. N. Q. Nguyen, J. Bryant, E. Noone, S. Bradshaw, M. Finn, M. Dunne, A. M. Shannon, J. Armstrong, A. D. Meade, F. M. Lyng, *Ther. Adv. Med. Oncol.* **2020**, *12*, 175883592091849.
- [43] A. Milani, M. Basirnejad, S. Shahbazi, A. Bolhassani, *Br. J. Pharmacol.* **2017**, *174*, 1290.
- [44] A. Mahadevan-Jansen, R. Richards-Kortum, *J. Biomed. Opt.* **1996**, *1*, 31.

**How to cite this article:** S. J. van Breugel, I. Low, M. L. Christie, M. R. Pokorny, R. Nagarajan, H. U. Holtkamp, K. Srinivasa, S. Amirapu, M. K. Nieuwoudt, M. C. Simpson, K. Zargar-Shoshtari, C. Aguergeray, *J. Biophotonics* **2023**, e202200334. <https://doi.org/10.1002/jbio.202200334>